6th Edition of the European Conference on Supercritical CO_2 (sCO_2) for Energy Systems
April 09–11, 2025, Delft, Netherlands

2025-sCO2.eu-201

A CASE STUDY OF USING SCO2 EQUIPMENT IN DIFFERENT GEOTHERMAL ENERGY SYSTEMS: AGS, EGS AND CPG

Morteza Esmaeilpour*
Chair of Geothermal Energy and Geofluids, Department of Earth and Planetary Sciences, ETH Zurich
Zurich, Switzerland
morteza.esmaeilpour@eaps.ethz.ch

Christopher Schifflechner
Chair of Energy Systems, School of Engineering and Design, Technical University of Munich
Munich, Germany

Nicolas Rangel Jurado
Chair of Geothermal Energy and Geofluids, Department of Earth and Planetary Sciences, ETH Zurich
Zurich, Switzerland

Tsubasa Onishi
Chair of Geothermal Energy and Geofluids, Department of Earth and Planetary Sciences, ETH Zurich
Zurich, Switzerland

Daniel Pokras
Chair of Geothermal Energy and Geofluids, Department of Earth and Planetary Sciences, ETH Zurich
Zurich, Switzerland

Jasper de Reus
Chair of Geothermal Energy and Geofluids, Department of Earth and Planetary Sciences, ETH Zurich
Zurich, Switzerland

Sebastian Köhlert
MAN Energy Solutions Schweiz AG
Zurich, Switzerland

Martin O. Saar
Chair of Geothermal Energy and Geofluids, Department of Earth and Planetary Sciences, ETH Zurich
Zurich, Switzerland

ABSTRACT
Climate change necessitates innovative solutions for producing clean energy and decreasing atmospheric CO_2 levels. Using CO_2 as a working fluid in geothermal applications is a smart strategy to achieve this goal, as it has the potential to outperform conventional water-driven geothermal systems in terms of power produced, and for some cases, simultaneously increase the amount of CO_2 that can be geologically sequestered. Power plant technology plays an important role in maximizing the value of geothermal resources. This is achieved through versatile power plant components that, barring large differences in CO_2 purity, can operate across various geothermal systems. This research compares the use of similar power plant components and technologies across various types of CO_2-based geothermal energy systems: hydrothermal systems with CO_2 as a secondary working fluid, Advanced Geothermal Systems (AGS), Enhanced Geothermal Systems (EGS), and CO_2-Plume Geothermal (CPG) systems. After providing ranges in possible operating conditions of these systems, the study employs TANGO (Techno-economic Analysis of Geo-energy Operations) to calculate the extracted energy and the Levelized Cost of Electricity (LCOE) for an example AGS, EGS, and CPG project, each with 10 MWe installed capacity. The findings indicate that CO_2 is an effective geothermal working fluid and that most CO_2 equipment can be used across the different geothermal systems. Given the extensive drilling required for AGS, LCOEs of CPG and EGS were found to be more competitive at current well construction costs.

1. INTRODUCTION

The transition to clean and renewable energy is essential for addressing climate change and ensuring global energy security. Among the renewable energy options, geothermal energy stands out as a clean, reliable, and sustainable alternative to fossil fuels. By harnessing the Earth's natural heat, geothermal energy provides a constant and stable power supply, unlike intermittent sources such as wind and solar. Its versatility allows for both electricity generation and direct heating applications, making it a critical solution for reducing carbon emissions across multiple sectors. As nations strive toward carbon neutrality, geothermal energy is increasingly recognized as a cornerstone of the green energy transition.

Understanding the diverse categories of geothermal systems is key to unlocking their full potential. These systems include hydrothermal (1,2), Enhanced Geothermal Systems (EGS) (3–

 DOI: 10.17185/duepublico/83331

5), Advanced Geothermal Systems (AGS) (6–9), low-temperature systems (10,11), and CO_2-Plume Geothermal (CPG) systems (12–15). Hydrothermal systems, which rely on naturally occurring reservoirs of hot water or steam, are the most established. EGS extends geothermal energy's scope by creating reservoirs in hot rock formations where natural permeability or water is insufficient. AGS takes this further with engineered technologies such as closed-loop systems to extract heat without directly using water or tapping natural reservoirs, enabling deployment in diverse geological settings. CPG systems utilize supercritical CO_2 as the working fluid, offering the dual benefits of higher efficiency and potential carbon sequestration. Meanwhile, low-temperature systems primarily serve direct heating purposes, such as heating buildings and greenhouses. Together, these systems provide a wide array of solutions for leveraging geothermal energy to meet growing energy demands.

CO_2-based geothermal systems are particularly noteworthy due to their innovative approach to energy production. By using CO_2 instead of water, these systems, including CPG, benefit from the fluid's high mobility, which enhances heat extraction from subsurface reservoirs. This design not only improves energy efficiency but also enables dual environmental and energy benefits by generating power while capturing and storing CO_2 in the subsurface. With these advantages, CO_2-based systems demonstrate significant potential for making geothermal energy both more efficient and environmentally sustainable.

Despite these advancements, geothermal energy adoption remains limited primarily due to high development costs (16,17). These expenses present a significant barrier, particularly in comparison to other renewables and fossil fuels. Reducing these costs is essential for geothermal energy to compete and scale globally. Advances in drilling techniques, reservoir engineering, and permitting processes play a vital role in overcoming financial challenges. Lowering costs would not only make geothermal energy more accessible to a wider range of regions but also stimulate investment and drive innovation, solidifying geothermal energy as a critical component of the renewable energy mix.

Cost reduction can be achieved through the development of innovative power plant technologies that enable shared infrastructure across geothermal systems (18). However, the presence of impurities in CO_2-based systems poses significant challenges to this shared usage. Impure CO_2 in geothermal steam can severely affect the performance and durability of surface plant components, particularly the turbine. It decreases turbine efficiency by altering the thermodynamic properties of the working fluid, leading to a reduced enthalpy drop and lower power output. Furthermore, CO_2 impurities increase corrosion and scaling, particularly in turbine blades, piping, and heat exchangers, resulting in faster equipment degradation and higher maintenance costs. Over time, these issues can lead to frequent shutdowns, reduced plant availability, and increased operational expenses.

Despite these challenges, new technologies and advanced facilities are being designed to handle both pure and impure CO_2, making them adaptable to various geothermal applications, including Enhanced Geothermal Systems (EGS), Advanced Geothermal Systems (AGS), hydrothermal systems with CO_2-secondary cycles, and CO_2 Plume Geothermal (CPG) systems. By sharing standardized equipment such as turbines, heat exchangers, and CO_2 management systems, these power plants significantly reduce both capital and operational expenses. Moreover, their ability to process impure CO_2 broadens the range of exploitable geothermal resources, further enhancing efficiency and cost-effectiveness. This shared infrastructure represents a transformative solution for making geothermal projects more economically viable and scalable. The primary novelty of this study lies in the quantification of the contribution of the surface plant and shared equipment to the total cost of a geothermal project and its impact on the levelized cost of electricity.

In this study, we numerically model geothermal systems that could benefit from this innovative power plant technology. Advanced numerical tools are employed to simulate energy extraction from the subsurface and to couple it with surface plant designs tailored for each system. Four geothermal system categories—EGS, AGS, hydrothermal systems with a CO_2-secondary cycle, and CPG—are analyzed to compute their power output and the associated costs of energy production. A detailed cost breakdown highlights the contribution of the surface plant to the total cost, emphasizing the importance of shared equipment in reducing overall expenses. Through cost comparisons and recommendations for further reductions, this study provides valuable insights into the economic performance of these geothermal systems and offers actionable strategies for enhancing their cost-effectiveness. The findings underscore the role of innovation in advancing geothermal energy as a vital pillar of the green energy transition.

2. SYSTEM DESCRIPTION

This study primarily focuses on the use of CO_2 as a working fluid, both in subsurface geothermal systems and surface power plants. The analysis encompasses four main types of geothermal systems: AGS, CPG, EGS, and hydrothermal systems.

2.1. ADVANCED GEOTHERMAL SYSTEMS (AGS)

Advanced Geothermal Systems (AGS) represent an innovative approach to geothermal energy that utilizes closed-loop systems to extract heat from the Earth's subsurface without the need for fluid interaction with underground reservoirs. This design eliminates the reliance on natural permeability and water availability, making AGS highly versatile and deployable in a broader range of geological settings compared to traditional hydrothermal or Enhanced Geothermal Systems (EGS). One of the key advantages of AGS is its environmental compatibility, as it minimizes the risk of induced seismicity and avoids

 DOI: 10.17185/duepublico/83331

contamination of groundwater. Additionally, AGS systems offer greater operational control, reducing uncertainties related to reservoir management and long-term productivity. However, the primary drawback of AGS lies in the high cost of drilling and well construction, which remains a significant barrier to widespread adoption. The need for advanced drilling technologies and materials to access deep geothermal resources can lead to substantial upfront investment, posing challenges for economic feasibility despite the system's technical benefits.

The use of CO_2 as a working fluid in Advanced Geothermal Systems (AGS) provides notable advantages for both the subsurface and surface components of the system. The superior inverse kinematic viscosity of CO_2, as well as its density's sensitivity to temperature changes, enhance the thermosiphon effect, improving the natural circulation of the fluid within the closed-loop system. On the surface side, the extracted hot CO_2 can be directly delivered to the power plant, serving simultaneously as a heat carrier and a working fluid for power generation (Figure 1). This direct utilization eliminates the need for intermediate heat exchangers, simplifying system design and increasing overall efficiency. These combined attributes position CO_2 as an optimal working fluid for maximizing the performance of AGS while advancing sustainability objectives.

A key advancement in the design of Advanced Geothermal Systems is the integration of multiple horizontal loops, which substantially enhances both system performance and economic viability. By increasing the surface area in contact with the geothermal reservoir, these loops improve heat absorption per meter of the system, enabling more efficient thermal energy extraction. This innovation not only increases the system's thermal output but also lowers the cost of energy production by maximizing energy absorption relative to the system's length. In this study, configurations with 1, 6, and 10 horizontal loops are analyzed, as depicted in Figure 2, highlighting the scalability and efficiency gains achieved with additional loops. It should be noted that while added horizontal wellbores greatly enhance energy absorption, drilling such long wellbores and assembling the equipment is a significant challenge in constructing these systems.

2.2. CO_2-PLUME GEOTHERMAL (CPG) SYSTEMS

CO_2-Plume Geothermal systems are an emerging geothermal energy production technology that uses supercritical carbon dioxide (CO_2) as the working fluid instead of water. This approach leverages the high mobility of CO_2 to enhance heat extraction from subsurface reservoirs, improving the efficiency and performance of geothermal systems. Beyond energy generation, CPG systems offer dual environmental and energy benefits by capturing and storing CO_2 in the subsurface while producing power, at a larger CO_2 storage efficiency compared to CCS as CO_2 density and volumetric sweeps are higher (19).

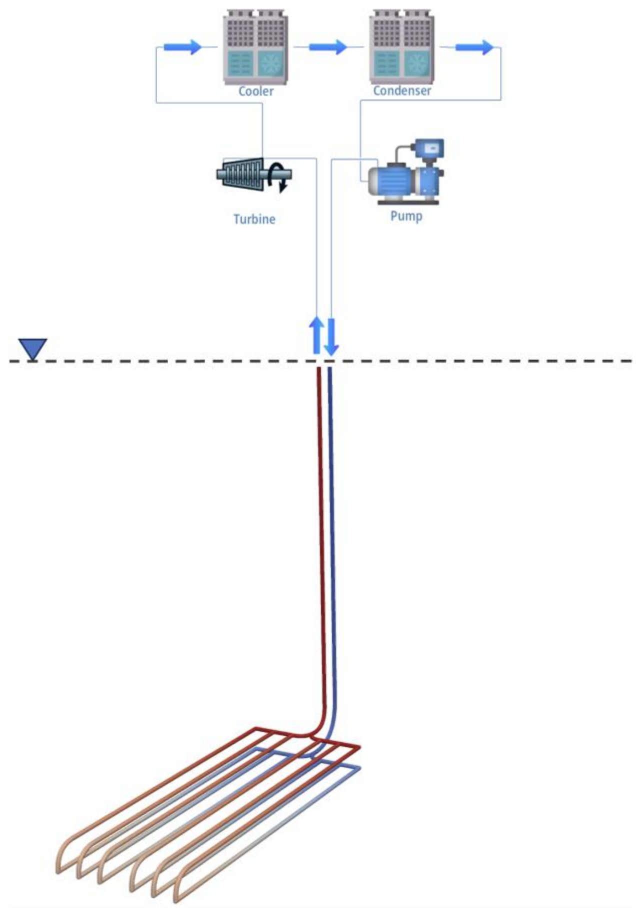

Figure 1. Schematic illustrating a multilateral AGS coupled to a surface plant for direct CO_2 utilization in electric power generation.

With advancements in power plant technology, these systems can even handle extracted impure CO_2, broadening their applicability and ensuring operational efficiency in diverse geological settings (Figure 3). The integration of carbon sequestration with renewable energy production positions CO_2-based geothermal systems, including CPG, as an innovative solution for achieving both efficient energy generation and environmental sustainability.

2.3. HYDROTHERMAL SYSTEMS WITH CO_2 AS A SECONDARY WORKING FLUID

Hydrothermal systems with CO_2 as a secondary working fluid represent a novel hybrid approach to geothermal energy production, integrating the conventional use of water for subsurface heat extraction with an innovative surface-level CO_2 cycle (Figure 4). In this configuration, water extracts heat from the geothermal reservoir, which is then transferred to a secondary surface cycle where CO_2 operates as a refrigerant. This design takes advantage of the unique thermodynamic properties of CO_2.

DOI: 10.17185/duepublico/83331

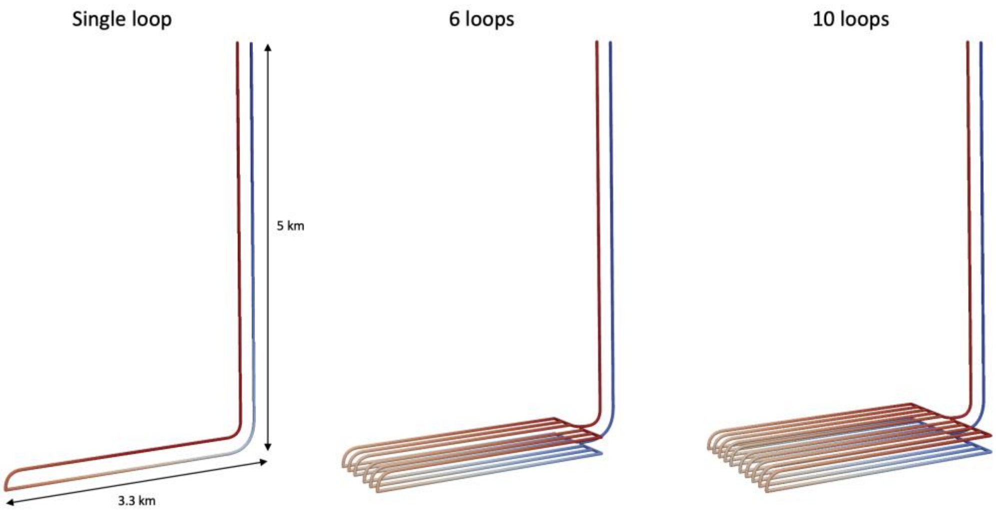

Figure 2. Schematic illustrating various AGS configurations with differing numbers of loops.

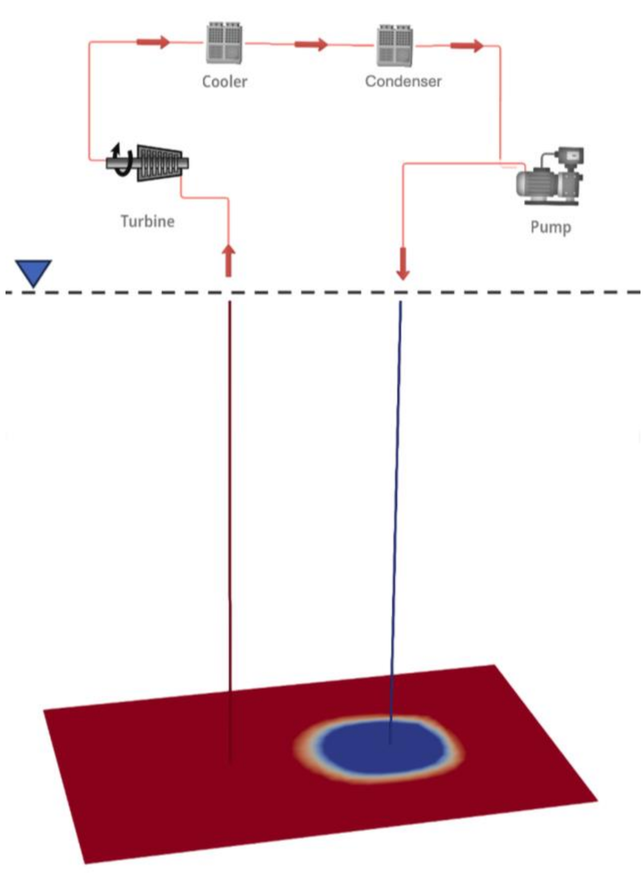

Figure 3. Schematic illustrating a CO_2-Plume Geothermal system coupled to a surface plant for direct CO_2 utilization in electric power generation.

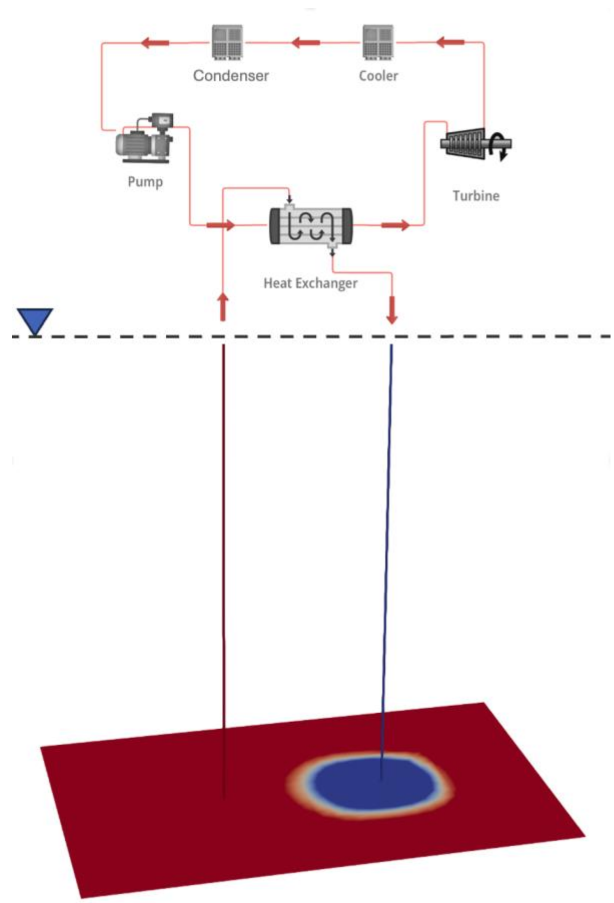

Figure 4. Schematic depicting a hydrothermal system coupled with a surface plant. The plant utilizes CO_2 as a refrigerant in a secondary cycle to generate electric power.

 DOI: 10.17185/duepublico/83331

2.4. ENHANCED GEOTHERMAL SYSTEMS (EGS)

Enhanced Geothermal Systems (EGS) utilizing CO_2 as the working fluid presents a transformative approach to geothermal energy production by integrating engineered geothermal reservoirs with the advantageous properties of CO_2. These systems create fractures in hot, impermeable rock to facilitate fluid flow and heat extraction. Replacing water with CO_2 enhances subsurface dynamics, as CO_2's superior mobility enables more efficient circulation through the reservoir, while its favorable thermodynamic properties allow for extracting significant amounts of heat energy (20). Beyond energy generation, this configuration provides the additional benefit of CO_2 sequestration, offering a dual-purpose solution that reduces greenhouse gas emissions. Furthermore, by minimizing water dependency, CO_2-based EGS open up possibilities for geothermal development in arid regions and provide a more environmentally adaptable alternative to traditional EGS designs, making them a forward-looking innovation in renewable energy technology.

3. NUMERICAL TOOLS AND METHODOLOGY

Since no single tool can simulate all types of geothermal systems, various tools are used for the simulations of this study.

3.1. MOSKITO

Modeling Advanced Geothermal Systems (AGS) requires the accurate simulation of coupled physical processes such as fluid flow, heat transfer, and thermodynamic changes in the subsurface environment. MOSKITO (21,22), a finite element code developed within the MOOSE framework, has proven to be a powerful tool for this purpose. It solves complex partial differential equations (PDEs) that govern mass, momentum, and energy conservation, allowing for the detailed representation of heat and fluid flow in AGS. Integrating GENEOS—a machine learning-based Equation of State (EOS)—into MOSKITO enhances its capability to compute thromo-physical properties of the fluid fast and accurately (23).

The governing equations for AGS modeled with MOSKITO are derived from fundamental conservation laws. The continuity equation for mass conservation is expressed as:

$$\frac{\partial \rho}{\partial t} + \frac{\partial}{\partial z}(\rho v) + m = 0 \tag{1}$$

where ρ is fluid density, v is velocity, and m accounts for sources or sinks of mass. The momentum equation captures the effects of pressure gradients, friction, and gravity:

$$\frac{\partial P}{\partial z} = \rho g \cos(\theta) \pm f \frac{\rho v^2}{2d} \pm \left(\frac{\partial}{\partial t}(\rho v) + \frac{\partial}{\partial z}(\rho v^2) \right) \tag{2}$$

where P is pressure, g is gravitational acceleration, θ is the inclination angle, f is the friction factor, and d is the wellbore hydraulic diameter. The energy equation models heat transfer processes, including convective and conductive contributions:

$$\frac{\partial}{\partial t}\left[\rho\left(h - \frac{P}{\rho} + \frac{1}{2}v^2\right)\right] - \frac{\partial}{\partial z}\left[\rho v\left(h + \frac{1}{2}v^2\right)\right] + \rho g \cos(\theta)\frac{Q}{A} + Q = 0 \tag{3}$$

where h is the specific enthalpy, Q accounts for heat sources/sinks, and A is the cross-sectional area of flow.

In addition to these, the lateral heat transfer equation models the heat exchange between the fluid and the surrounding formation. This is crucial for capturing the thermal interaction of the wellbore system with the geologic environment:

$$q = 2\pi r_o U_T \left(T_f - T_g\right) \tag{4}$$

where r_o is the outer radius of the tubing, U_T is the overall heat transfer coefficient, T_f is the fluid temperature, and T_g is the formation temperature. This equation accounts for the conductive and convective heat loss or gain across the wellbore casing and the surrounding formation.

3.2. CMG

Computer Modelling Group (CMG) software provides a robust platform for simulating Enhanced Geothermal Systems (EGS), offering advanced capabilities for modeling fluid flow, heat transfer, and geomechanical interactions within engineered reservoirs (24). CMG's compositional and thermal reservoir simulator GEM, can be used for solving coupled thermal-hydraulic processes in EGS. This includes multi-phase fluid flow and the interactions between the reservoir rock and the injected working fluids (e.g., water, CO_2, or brine).

The simulation of EGS in CMG is governed by the principles of mass, momentum, and energy conservation, which are mathematically represented as follows:

Mass Conservation (Continuity Equation):

$$\frac{\partial(\phi\rho)}{\partial t} + \nabla \cdot (\rho \mathbf{v}) = q_m \tag{5}$$

where ϕ is the porosity, ρ is the fluid density, $\mathbf{v}$ is the velocity vector, and q_m represents mass sources or sinks (e.g., injection or production wells). This equation ensures that fluid mass is conserved as it flows through the porous medium.

Momentum Conservation (Darcy's Law):

$$\mathbf{v} = -\frac{k}{\mu}(\nabla P - \rho g \nabla z) \tag{6}$$

 DOI: 10.17185/duepublico/83331

where k is the permeability tensor, μ is the fluid viscosity, P is the pressure, g is the gravitational acceleration, and ∇z accounts for depth changes. Darcy's law governs fluid flow in porous media, incorporating pressure gradients and gravitational effects.

Energy Conservation (Heat Transport):

$$\frac{\partial}{\partial t}\left(\phi\rho c_f T + (1-\phi)\rho_r c_r T\right) + \nabla\cdot\left(\rho c_f \mathbf{v}T - k_T\nabla T\right) = Q_h \quad (7)$$

where T is the temperature, c_f and c_r are the specific heat capacities of the fluid and rock, respectively, ρ_r is the rock density, k_T is the thermal conductivity tensor, and Q_h represents heat sources or sinks. This equation captures the transfer of heat by conduction, convection, and thermal interactions between fluid and rock.

3.3. TANGO

The subsurface modeling of AGS, CPG, EGS, and hydrothermal systems is seamlessly integrated with the design of surface plants using a tool named TANGO (Techno-economic ANalysis of Geoenergy Operations). TANGO provides a modular platform to represent all surface and subsurface components, including the wellbore, reservoir, and power plant. These components can be modeled using either simple analytical approaches or advanced external software, such as MOSKITO and CMG, to capture more detailed system dynamics. The tool supports both fully coupled and weakly coupled configurations, offering flexibility based on the required modeling precision.

In addition to its modeling capabilities, TANGO computes all the associated costs of a geothermal system, including drilling, exploration, stimulation, permitting, surface gathering, and surface power plant expenses (25). It also calculates the levelized cost of electricity (LCOE) and heat, providing critical insights into the economic feasibility of geothermal projects. Furthermore, TANGO offers flexibility in optimization, enabling users to explore various design and operational scenarios to minimize costs and maximize efficiency.

In this study, MOSKITO and CMG are employed for detailed subsurface modeling of AGS and EGS, respectively, to ensure accurate simulation of thermal, hydraulic, and geomechanical processes. For CPG and hydrothermal systems, TANGO's built-in analytical models are implemented to provide an efficient representation of subsurface and surface interactions. The surface plant design within TANGO is powered by the TesPy Python library, enabling modular and flexible modeling of plant components to adapt to various system designs and operating conditions.

4. RESULTS

4.1. ADVANCED GEOTHERMAL SYSTEMS (AGS)

The first system evaluated in this study is the Advanced Geothermal System (AGS). The behavior of fluid flow and heat transfer in these systems has already been evaluated in previous studies conducted by the authors of this study (6–9). It has been demonstrated that AGS systems can operate effectively using the thermosiphon effect over extended periods (9). This stability arises from the significant temperature difference between the vertical wellbores in the system. It was also shown that under specific conditions, not only does temperature breakthrough (a sudden drop in extraction temperature) not occur, but the extraction temperature can even increase over time as the area around the production well heats up, thereby minimizing energy loss. Although the evaluated AGS system in those studies was capable of producing approximately 2 MW of thermal power, the high cost associated with long wellbores resulted in elevated energy expenses. In another study, the authors showed that using a multi-lateral well system could reduce the ratio of total wellbore length to produced thermal power, improving efficiency (8). However, the potential of AGS systems for electric power generation and the associated levelized cost of energy were not addressed in those studies. These aspects will be the focus of the present study.

The AGS configurations analyzed in this study have a vertical depth of 5 km and a horizontal extension of 3.3 km, as shown in Figure 2. The borehole diameter is 0.4 m for both the vertical and horizontal sections. The vertical wellbores are cased with a 3 cm thick casing and cemented with a 4 cm thick layer, while the horizontal wellbores are directly exposed to the surrounding hot formation. The thermo-physical properties of the formation, casing, and cement layer are provided in Table 1. For the analysis, the average annual surface temperature is assumed to be 10°C, and the subsurface temperature gradient is 30°C/km. Initially, the fluid within the borehole system is considered to be in thermal equilibrium with the surrounding formation. The hydrostatic pressure at depth serves as the initial condition. The single-loop AGS is modeled with a flow rate of 20 L/s. The boundary conditions for pressure and temperature are derived from the power plant model.

The extracted hot CO_2 flows through a turbine with an isentropic efficiency of 0.78, where its pressure decreases to 7 MPa. If the CO_2 remains in a single-phase state at the turbine outlet, it passes through a cooler to reach a saturated gas state. The saturated gas then enters a condenser to produce saturated liquid. However, if the CO_2 exits the turbine in a two-phase state, the cooler stage is excluded, and the fluid moves directly to the condenser. The saturated liquid is then pressurized using a pump with an efficiency of 0.9, if necessary. If the thermosiphon effect is insufficient to maintain fluid circulation, the pump outlet state is used as the inlet boundary condition for the subsurface AGS model. Otherwise, the fluid state at the condenser outlet serves as the boundary condition. The simulations are conducted over 20 years of operation. To evaluate the economic feasibility of the system, the same 20-year payback period is considered, with an interest rate of 9.5%. The levelized cost of electricity (LCOE) is computed based on these assumptions.

 DOI: 10.17185/duepublico/83331

Table 1. Thermo-physical properties of formation, casing, and cement layer (AGS modeling)

Formation density	Formation heat capacity	Formation thermal conductivity	Cement thermal conductivity	Casing thermal conductivity	Subsurface temperature gradient	Average annual surface temperature	Roughness
$kg{\cdot}m^{-3}$	$J{\cdot}kg^{-1}{\cdot}K^{-1}$	$W{\cdot}m^{-1}{\cdot}K^{-1}$	$W{\cdot}m^{-1}{\cdot}K^{-1}$	$W{\cdot}m^{-1}{\cdot}K^{-1}$	$°C{\cdot}km^{-1}$	°C	m
2200	850	3	0.7	43.75	30	10	0.0001

Figure 5 and Figure 6 illustrate the power generation and consumption across the surface plant components of the single-loop AGS. The results indicate that, for all evaluated cases, the thermosiphon effect is sufficiently robust to support operating flow rates between 10 and 30 L/s. Consequently, no pumping is required, which represents a significant operational advantage of AGS systems. Another notable finding is that in all simulated cases, the expanded fluid exiting the turbine is in a two-phase state. This eliminates the need for cooling, simplifying system design and reducing operational complexity. As a result, the condenser is the only power-consuming component within the power plant. Both turbine power generation and condenser power consumption increase with the flow rate. However, as shown in Figure 6, the net power output consistently increases as the flow rate rises. An additional critical result is the stability of power generation over time, a key factor for the reliability of geothermal systems. This stability is attributed to two primary factors. First, the heat extraction mechanism is governed solely by conduction, which limits the cooled area around the wellbore system. Second, the relatively low flow rates ensure controlled energy extraction from the reservoir. As a result, no temperature or power breakthroughs are observed, further enhancing system reliability.

The relatively low flow rate results in modest electric power generation, while the construction of a long wellbore system at significant depths incurs high costs, substantially increasing the total capital expenditure (CAPEX) of the geothermal project. Consequently, the calculated LCOEs for the designed single-loop AGS systems range from 2.64 to 7.7 $/kWh, as shown in Table 2. Increasing the flow rate and incorporating multiple loops in the horizontal section are the proposed strategies for reducing LCOE values and improving the overall economic viability of AGS systems.

To assess the impact of additional loops on the economic viability of AGS systems, two configurations with 6 and 10 loops were designed. The base single-loop system operates with a flow rate of 20 L/s, while the flow rates for the multilateral configurations are determined by multiplying the number of loops by 20 L/s. Accordingly, flow rates of 120 L/s and 200 L/s are considered for the 6-loop and 10-loop AGS systems, respectively. These higher flow rates enhance power generation in multilateral AGSs, enabling them to approach their maximum energy extraction capacity.

As shown in Figure 7, there is an initial drop in turbine power generation. This occurs during an initial period when the cooled area around the wellbore system expands due to conduction. After this phase, the extraction temperature and power generation stabilize as the cooled area ceases to expand significantly. Simulations reveal that for the 10-loop AGS operating at a flow rate of 200 L/s, stable power generation consistently exceeds 3 MW (Figure 8). Over the 20-year project lifetime, the average power generation for this configuration is approximately 3.5 MW, demonstrating the potential of multilateral AGS designs to deliver significant and reliable energy output.

A comparison of Table 2 and Table 3 clearly demonstrates the success in reducing the levelized cost of electricity by implementing multilateral AGS systems operating at higher flow rates. This reduction is achieved by increasing the energy absorption per meter of the system. While both higher flow rates and longer well lengths contribute to higher total CAPEX, the enhanced energy absorption surpasses the additional costs, ultimately resulting in lower LCOE values. Despite this progress, the achieved LCOE remains an order of magnitude higher than the desired target. However, advancements in drilling technologies, such as plasma drilling, hold the potential to significantly lower drilling costs. With such innovations, AGS systems could emerge as a transformative technology within the geothermal sector.

To achieve the goal of designing power plant units with a capacity of approximately 10 MW, it is necessary to operate multiple AGS systems in parallel. Given that the 10-loop AGS demonstrates a superior LCOE compared to other configurations, we recommend utilizing three such systems. This arrangement would yield an estimated total electric power output of approximately 10.5 MW, aligning well with the desired capacity target.

DOI: 10.17185/duepublico/83331

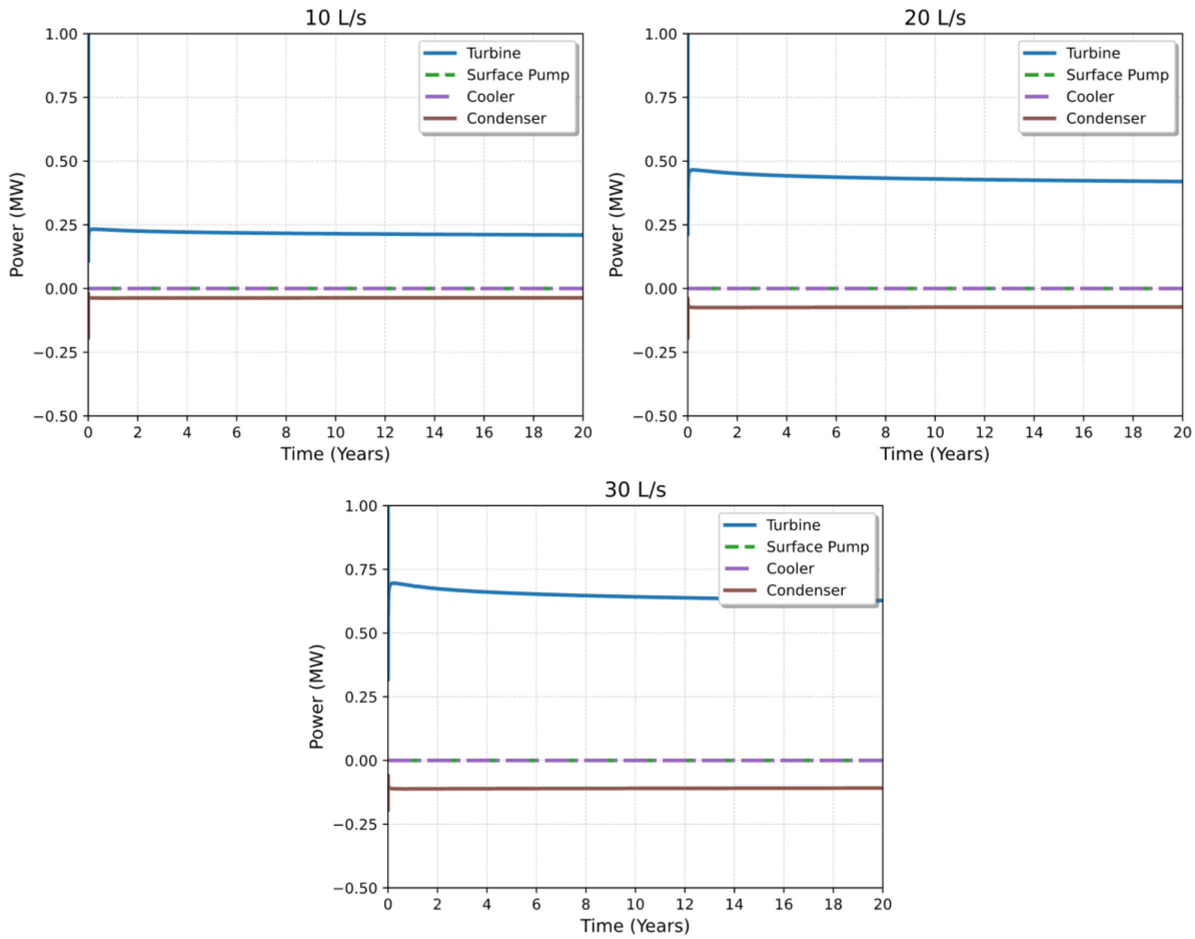

Figure 5. Power generation and consumption across surface plant components over time, analyzed for different flow rates in the single-loop AGS.

Table 2. Key performance indicators for single-loop AGSs operating with different flow rates.

Flow rate (L/S)	Well CAPEX ($)	Permitting Capex ($)	Exploration CAPEX ($)	Surface gathering CAPEX ($)	Surface plant CAPEX ($)	Total CAPEX ($)	Net Electricity (KW)	LCOE ($/kWh)	SpCC ($/kW)
10	64786395	1478867	881721	341111	1436468	68924563	179.90	7.70	383129
20	64786395	1478867	881721	341111	2403911	69892006	359.76	3.91	194274
30	64786395	1478867	881721	341111	3242431	70730526	537.47	2.65	131599

 DOI: 10.17185/duepublico/83331

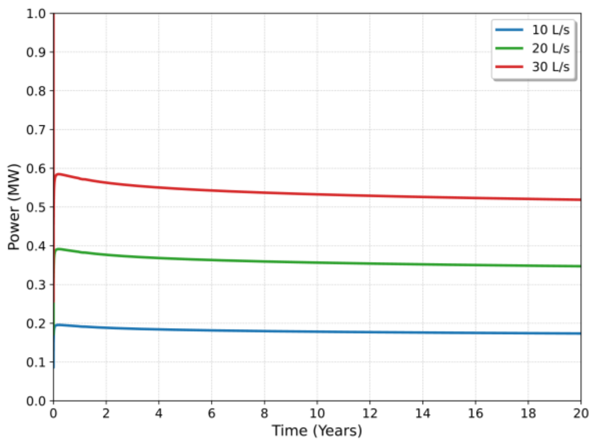

Figure 6. Net electric power generated over time for various flow rates in the single-loop AGS.

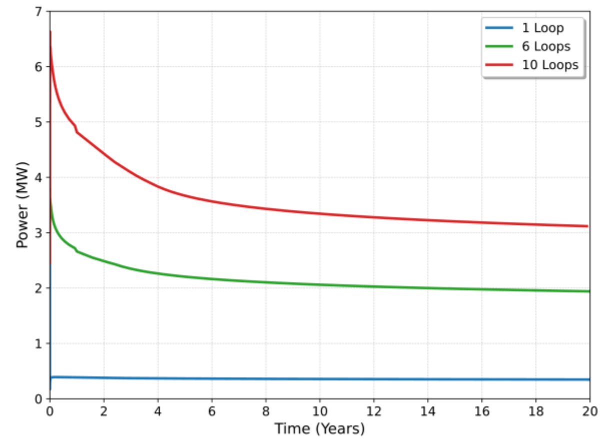

Figure 8. Net electric power generated over time for various AGS configurations addressed in Figure 2. The operating flow rates for the cases with 1, 6, and 10 loops are 20 L/s, 120 L/s, and 200 L/s, respectively.

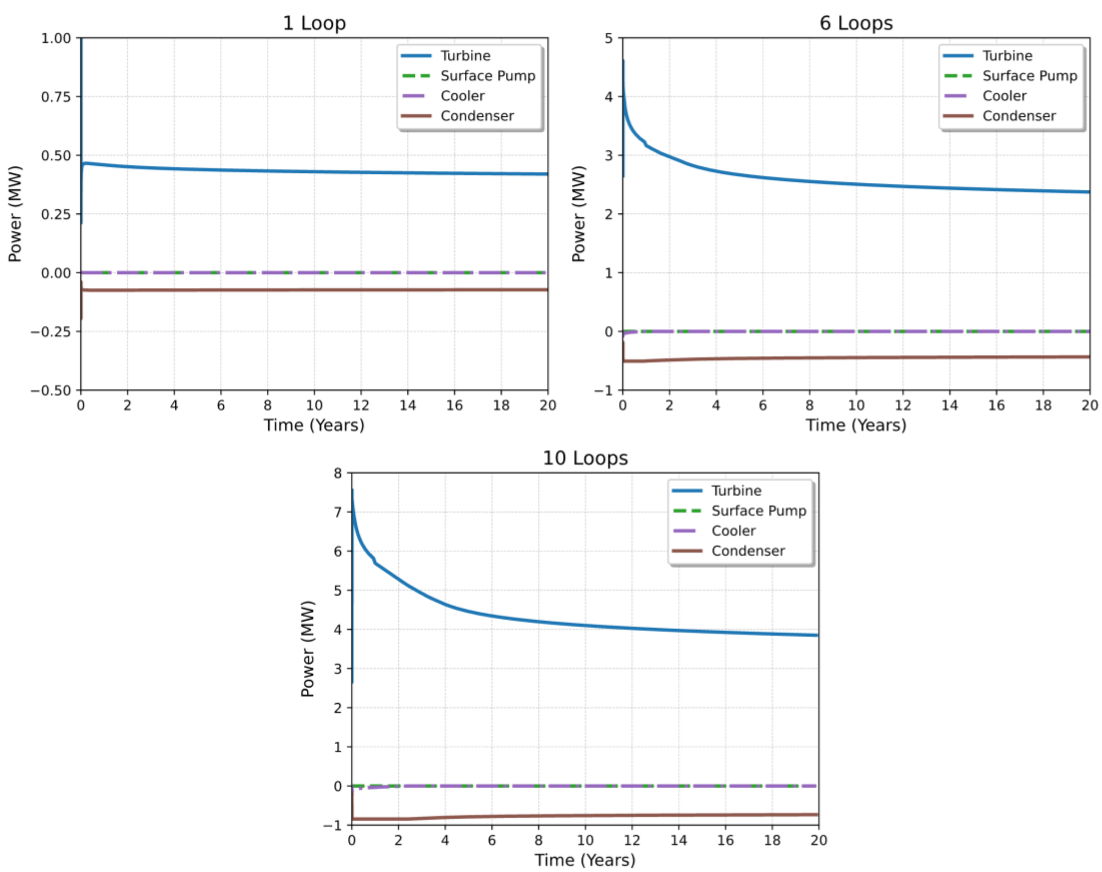

Figure 7. Power generation and consumption across surface plant components over time, analyzed for AGS configurations addressed in Figure 2. The operating flow rates for the cases with 1, 6, and 10 loops are 20 L/s, 120 L/s, and 200 L/s, respectively.

DOI: 10.17185/duepublico/83331

Table 3. Key performance indicators for various AGS configurations addressed in Figure 2. The operating flow rates for the cases with 1, 6, and 10 loops are 20 L/s, 120 L/s, and 200 L/s, respectively.

Number of loops	Well CAPEX ($)	Permitting Capex ($)	Exploration CAPEX ($)	Surface gathering CAPEX ($)	Surface plant CAPEX ($)	Total CAPEX ($)	Net Electricity (KW)	LCOE ($/kWh)	SpCC ($/kW)
1	64786395	1478867	881721	341111	2403911	69892006	359.76	3.91	194274
6	185269654	1478867	881721	341111	9302434	197273787	2154.43	1.84	91566
10	274044902	1478867	881721	341111	13675904	290422505	3510.54	1.66	82728

4.2. HYDROTHERMAL SYSTEMS

The second system evaluated in this study is a hydrothermal system integrated with a CO_2-based secondary cycle. As previously mentioned, the core concept involves using a heat exchanger at the surface level to transfer heat from water circulating in the subsurface to CO_2, which acts as the working fluid in the secondary cycle. This approach allows for leveraging existing CO_2-handling infrastructure while maintaining water circulation in the subsurface. For this model, a five-spot pattern is utilized, consisting of four injection wellbores at the corners and a single production wellbore at the center with a well spacing of 707 m. The system is assumed to have a depth of 5 km, with wellbores having a diameter of 31 cm. The relevant thermophysical properties, the average annual surface temperature, and subsurface temperature gradient are detailed in Table 4. Initially, the wellbores are assumed to be in thermal equilibrium with the surrounding formation, and the hydrostatic condition is applied to set the initial fluid pressure.

In the secondary cycle, the flow rate of CO_2 is adjusted to maintain a pinch temperature of 7°C in the heat exchanger, given the known inlet pressure and temperature of CO_2. A pump is used to increase the CO_2 pressure, and its temperature is raised as it passes through the heat exchanger. The hot, pressurized CO_2 then flows through a turbine with an isentropic efficiency of 78%, where its pressure decreases to the saturation pressure of CO_2 (at the average annual surface temperature plus the pinch temperature). Similar to the AGS system, if the expanded CO_2 has a temperature above the saturation point, a cooler is used to reduce the temperature. Otherwise, the CO_2 bypasses the cooler and enters the condenser directly to produce saturated liquid. The liquid CO_2 is then pressurized using a pump with an isentropic efficiency of 0.9, preparing it for re-entry into the secondary cycle.

This hydrothermal system also incorporates a production submersible pump to address the limitations of water mobility, which is not as favorable as that of CO_2. As the thermosiphon effect is insufficient to support high flow rates, the production pump is installed at a depth of 1 km to pressurize the water if needed. It is assumed that the water pressure drop in the heat exchanger is negligible, and the subsurface hydrothermal system operates with an injection and extraction pressure of 4 MPa. Similar to the AGS system, an operational and payback period of 20 years, along with an interest rate of 9.5%, is used for the economic calculations.

The evaluation of a single five-spot hydrothermal system was conducted for four flow rates ranging from 15 to 60 kg/s. As shown in Figure 9, the thermosiphon effect is insufficient to support flow rates of 45 and 60 kg/s. Consequently, a downhole pump is required to maintain subsurface flow circulation, with its power consumption increasing as the operating flow rate rises. Over time, this power consumption further increases due to declining production pressure, a result of reservoir cooling. Conversely, the power required for cooling and condensing decreases over time. Both consumed and produced power exhibit an almost linear relationship with the flow rate. Net thermal power also increases with flow rate, as illustrated in Figure 10. It is important to note that while higher flow rates initially yield greater power generation, they accelerate thermal depletion of the reservoir. This leads to a more pronounced decline in produced power over time, emphasizing the trade-off between short-term gains and long-term sustainability in system performance.

A comparison of Table 5 and Table 2 reveals that the hydrothermal system achieves a lower LCOE compared to the AGS system. This is primarily due to its shorter well length and its ability to extract significant energy from the reservoir through both conduction and convection. Despite this advantage, the LCOE values yet remain higher than the desired target, and the amount of electricity produced is still significantly below the 10 MW capacity goal.

 DOI: 10.17185/duepublico/83331

Table 4. reservoir setting for hydrothermal system

Formation density	Formation heat capacity	permeability	porosity	Reservoir thickness	Subsurface temperature gradient	average annual surface temperature
kg·m⁻³	J·kg⁻¹·K⁻¹	m^2	-	m	°C·km⁻¹	°C
2650	1000	10^{-13}	0.1	100	35	15

The first strategy examined for scaling up power generation and reducing LCOE involves increasing the flow rate to a maximum of 150 kg/s, which is within the tolerance limits of the wellbore system. However, even at this high flow rate, the desired net power output of 10 MW is not achieved. To address this, multiple five-spot patterns are evaluated. Specifically, three configurations with grid patterns of [*nx*, *ny*] = [2, 2], [3, 3], and [4, 4] are analyzed.

In these configurations, achieving a net electric power of 10 MW is possible with a hot water flow rate lower than 150 kg/s, but this results in a high LCOE. To mitigate this, the flow rate is fixed at 150 kg/s, and multiple power plants, each with a capacity of approximately 10 MW, are implemented. This approach not only lowers LCOE but also maximizes power generation while enabling the use of existing geothermal power plant technology designed for capacities near 10 MW. Sensitivity analysis reveals that the CO_2 cycle achieves a net electric power of 10 MW when the hot water flow rate entering the heat exchanger is approximately 400 kg/s. Consequently, the number of power plants required for each five-spot pattern is determined using the formula:

$$\text{Number of Power Plants} = \text{int}\left[n_x \times n_y \times 150/400\right] + 1 \quad (9)$$

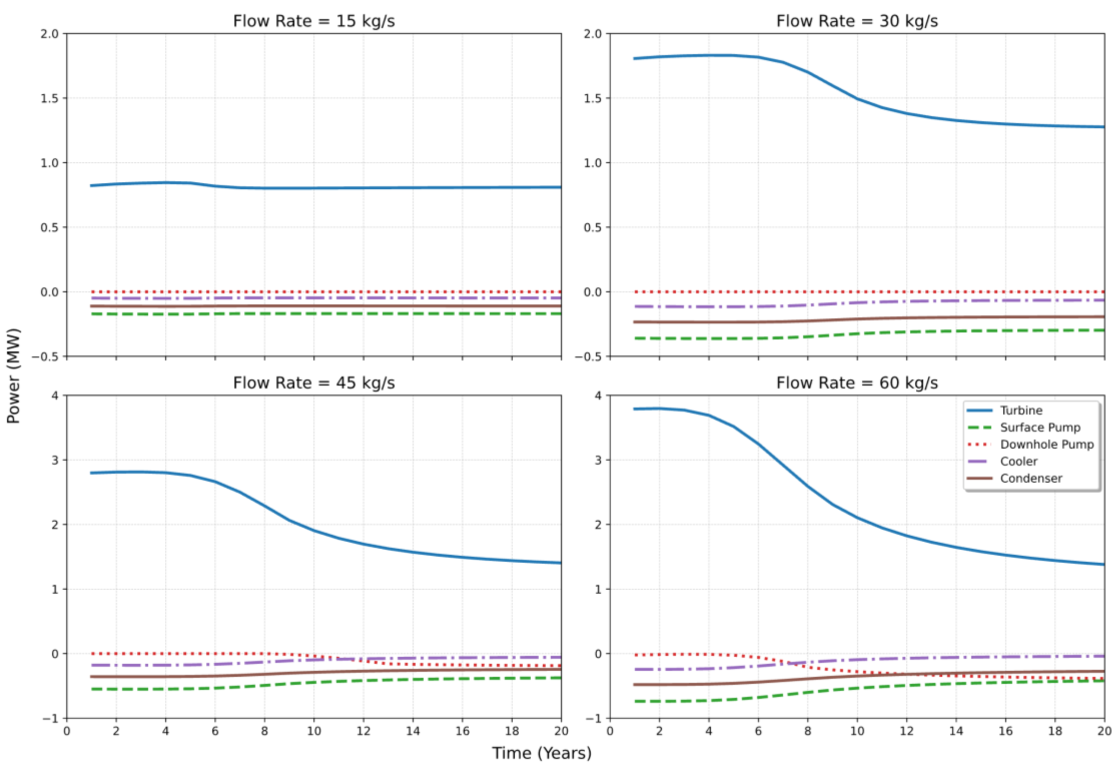

Figure 9. Power generation and consumption across surface plant components over time, evaluated for different flow rates. The CO_2 secondary cycle is coupled with a hydrothermal system that operates with water as a working fluid.

DOI: 10.17185/duepublico/83331

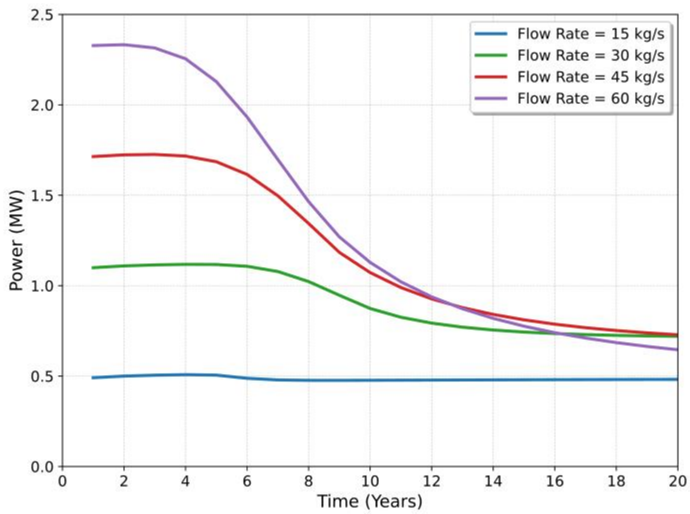

Figure 10. Net electric power, generated over time for various flow rates in a hydrothermal system coupled with a CO_2 secondary cycle.

Based on this formula, the required number of power plants is 2, 3, and 6 for the patterns [2, 2], [3, 3], and [4,4], respectively. The produced and consumed power for each designed power plant is shown in Figure 11 and Figure 12. The dominant power consumer in the system is the surface pump, which pressurizes the CO_2, followed by the condenser. While the generated net power does not always reach exactly 10 MW, the system is designed to approach this value while maintaining the water flow rate of 150 kg/s.

Table 6 demonstrates that increasing the number of five-spot patterns successfully reduces LCOE. For the [4,4] configuration, the LCOE reaches as low as 0.27 $/kWh. Observing the trend, it is reasonable to predict that further expansion of the model to include additional five-spot patterns could lead to lower LCOE values.

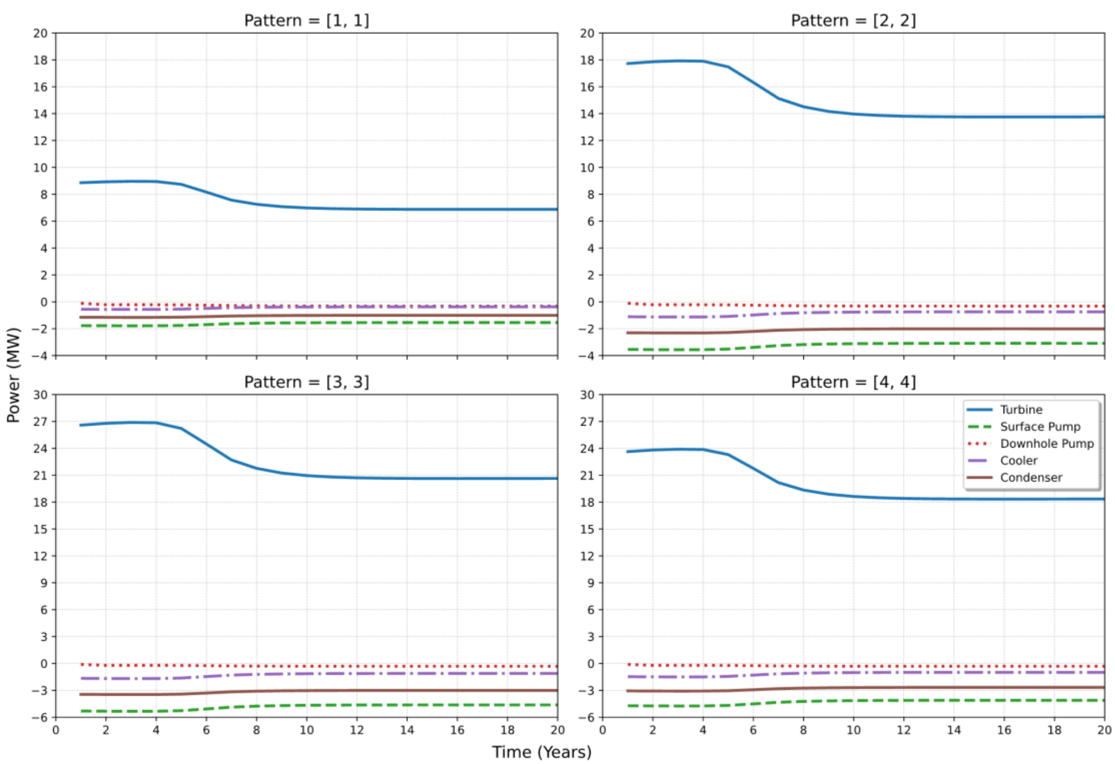

Figure 11. Power generation and consumption across surface plant components over time, evaluated for different five-spot patterns. In all cases, the same power plants work with different pattern-specific flow rates.

DOI: 10.17185/duepublico/83331

Table 5. Key performance indicators for hydrothermal systems coupled with a CO_2 secondary cycle, evaluated at various flow rates.

Flow rate (kg/S)	Well CAPEX ($)	Permitting Capex ($)	Exploration CAPEX ($)	Surface gathering CAPEX ($)	Surface plant CAPEX ($)	Total CAPEX ($)	Net Electricity (KW)	LCOE ($/kWh)	SpCC ($/kW)
15	36506133	1478867	881721	961560	3525138	43353421	485.15	1.80	89361
30	36506133	1478867	881721	961560	5624809	45453092	905.32	1.01	50206
45	36506133	1478867	881721	961560	7322516	47150799	1092.92	0.87	43141
60	36506133	1478867	881721	961560	8572512	48400795	1109.82	0.88	43611

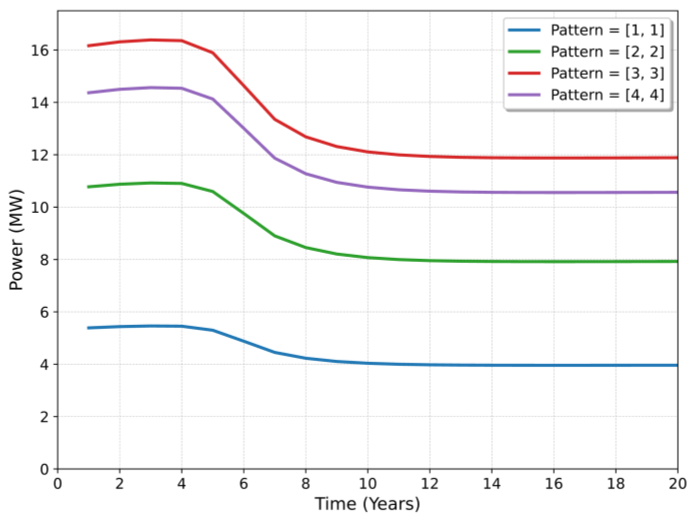

Figure 12. Net electric power of a single plant over time for various patterns in a hydrothermal system coupled with a CO_2 secondary cycle. The total thermal power is equal to the number of power plants multiplied by the net power of each power plant shown here.

4.3. CO_2-PLUME GEOTHERMAL (CPG) SYSTEMS

The third model evaluated in this study is the CO_2-Plume Geothermal (CPG) system. The subsurface setting of the CPG system closely resembles that of a hydrothermal system, while its surface plant configuration is similar to that of AGS. For economic calculations, the operation and payback period is assumed to span 20 years, with a fixed interest rate of 9.5%.

Similar to the hydrothermal system, the wellbores in five-spot CPG systems are assumed to be in thermal equilibrium with the surrounding formation, and a hydrostatic condition is applied to establish the initial pressure distribution. Figure 13 and Figure 14 illustrate the power generated and consumed by each component of the surface plant over time for varying flow rates. A key advantage of the CPG system compared to the simulated hydrothermal system is the stability of power generation over time. The higher mobility of CO_2 compared to water enhances the thermosiphon effect, resulting in higher extraction pressures. Moreover, the extracted hot CO_2 can be expanded in a turbine without the need for an intermediate heat exchanger, albeit co-produced brine does require liquid handling upstream of the turbine.

The calculated LCOEs for the CPG systems are lower compared to AGS systems. However, the comparison between CPG and hydrothermal systems is more nuanced. CPG systems tend to be more expensive due to the use of corrosion-resistant materials in both surface and subsurface facilities. This cost differential is evident when comparing Table 5 and Table 7. At lower flow rates, the hydrothermal system demonstrates a more favorable LCOE than the CPG system. Nevertheless, as the flow rate increases to 60 kg/s, the rate of power increase in the CPG system surpasses that of the hydrothermal system, which experiences a notable decline in power production. As previously discussed, this decline becomes more pronounced at higher flow rates, as shown in Figure 10. This behavior does not occur in the CPG system within this range of flow rates. Consequently, at a flow rate of 60 kg/s, the higher power generation of the CPG system offsets its higher costs, resulting in an equivalent LCOE to that of the hydrothermal system.

The LCOE values presented in Table 7 can be reduced by increasing the flow rate and expanding the number of five-spot patterns. The adjusted flow rates and the number of power plants were matched to those in the hydrothermal case. As depicted in Figure 15, the CPG system demonstrates notable advantages: it does not require downhole pumping, and the power consumption by the cooler is nearly zero. However, at a high flow rate of 150 kg/s, the thermosiphon effect alone is insufficient to maintain system operation, necessitating the use of pumps. The power consumed by the pump is nearly double that of the condenser. Although the higher flow rate significantly boosts turbine power generation, it also substantially increases pumping power requirements. Overall, the net power output rises with increasing flow rates, and as shown in Figure 16, the net power of the CPG system becomes comparable to that of the hydrothermal system.

DOI: 10.17185/duepublico/83331

Table 6. Key performance indicators for hydrothermal systems coupled with a CO_2 secondary cycle, evaluated for various patterns.

	Well CAPEX ($)	Permitting Capex ($)	Exploration CAPEX ($)	Surface gathering CAPEX ($)	Surface plant CAPEX ($)	Total CAPEX ($)	Net Electricity (KW)	LCOE ($/kWh)	SpCC ($/kW)
[1,1]	78875427	1478867	881721	3846243	18701750	103784010	4141.145	0.50	25061
[2,2]	205076112	1478867	881721	15384973	61734203	284555877	17123.092	0.33	16618
[3,3]	394377139	1478867	881721	34616189	124602476	555956393	38945.841	0.29	14275
[4,4]	646778508	1478867	881721	61539893	228564168	939243157	69050.880	0.27	13602

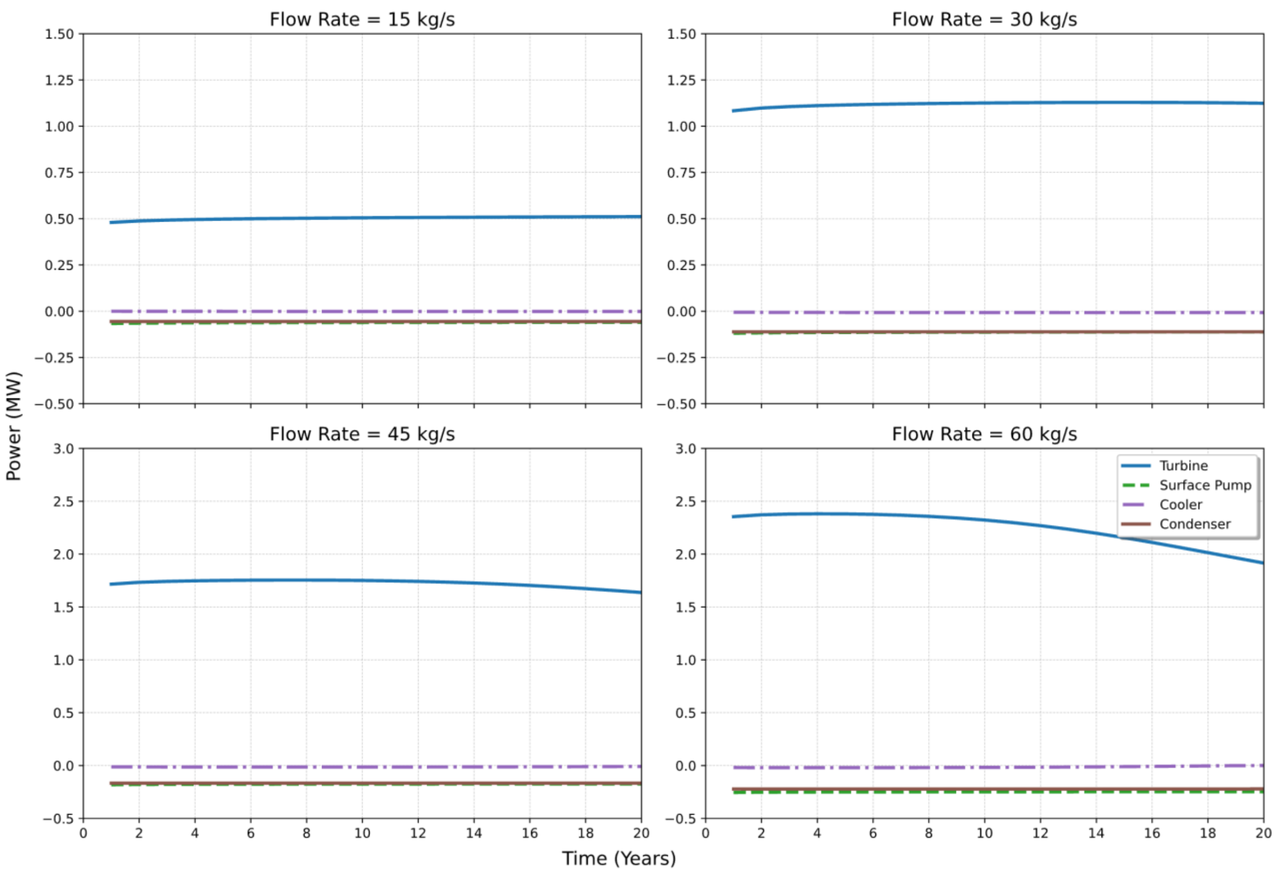

Figure 13. Power generation and consumption across surface plant components over time, analyzed for different flow rates in CO_2-Plume Geothermal systems

DOI: 10.17185/duepublico/83331

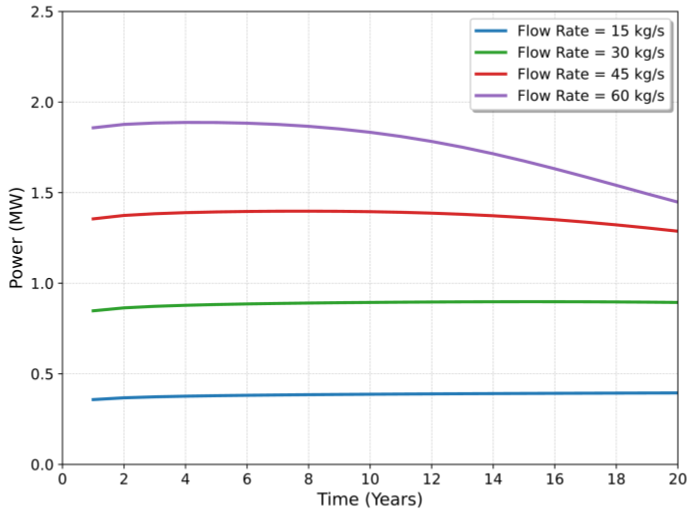

Figure 14. Net electric power generated over time for various flow rates in a CO_2-Plume Geothermal system.

Table 8 indicates that increasing the number of five-spot configurations reduces the LCOE. Nevertheless, despite achieving a comparable net power output to the hydrothermal system, the LCOE for the CPG system remains high. This difference arises from additional costs associated with corrosion-resistant materials, extended monitoring areas, and increased permitting and exploration costs. The CCS project underlying the CPG project would likely bear the latter. Sharing power plant facilities could lower the LCOE by lowering the cost of equipment, presenting an opportunity for cost optimization in future deployments of CPG systems. Additionally, the above evaluation does not incorporate the monetization of additional CO2 that can be stored compared to a baseline CCS project on which CPG was applied.

4.4. ENHANCED GEOTHERMAL SYSTEMS (EGS)

The final model evaluated in this study is the Enhanced Geothermal System (EGS) utilizing CO_2 as the working fluid.

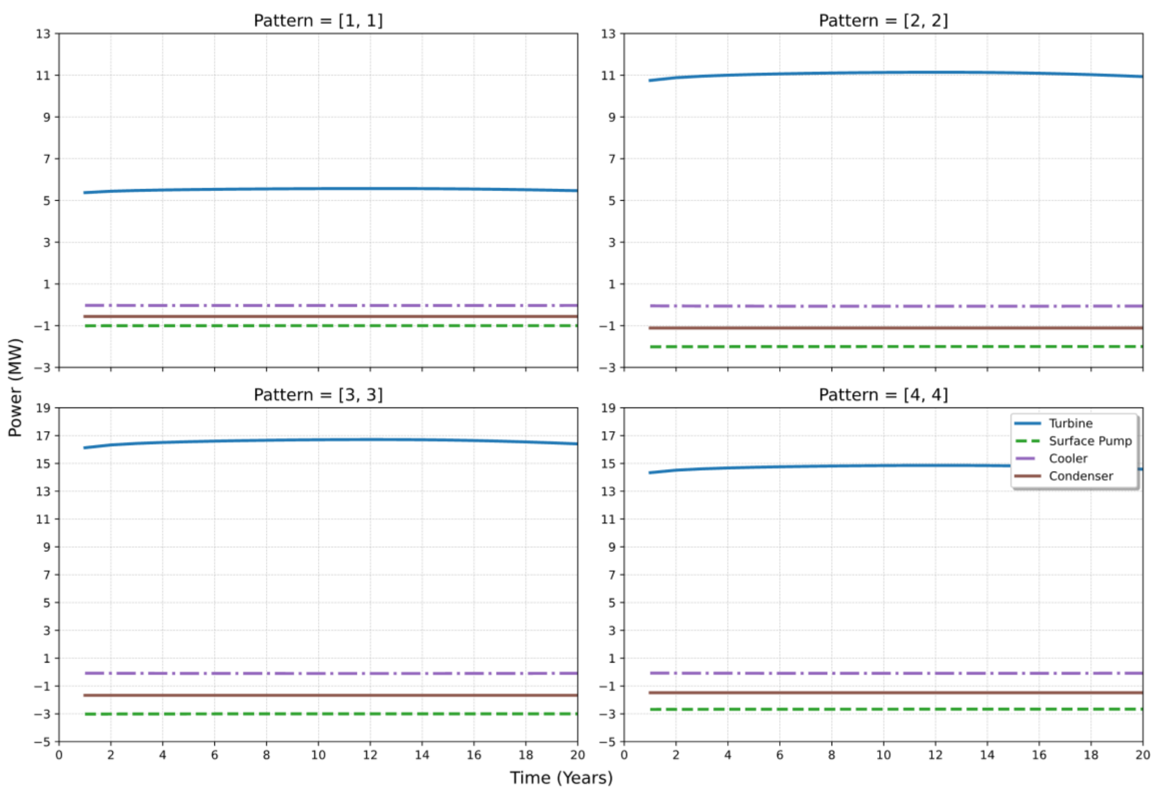

Figure 15. Power generation and consumption across surface plant components over time, evaluated for different five-spot patterns. In all cases, the same CPG plants work with different pattern-specific flow rates.

 DOI: 10.17185/duepublico/83331

Table 7. Key performance indicators for CO_2-Plume Geothermal systems operating with different flow rates.

Flow rate (L/S)	Well CAPEX ($)	Permitting Capex ($)	Exploration CAPEX ($)	Surface gathering CAPEX ($)	Surface plant CAPEX ($)	Total CAPEX ($)	Net Electricity (KW)	LCOE ($/kWh)	SpCC ($/kW)
15	43249423	15505491	8469968	961560	2731452	70917896	384.65	3.71	184371
30	43249423	15505491	8469968	961560	4699968	72886413	888.14	1.65	82065
45	43249423	15505491	8469968	961560	6414187	74600631	1368.86	1.10	54498
60	43249423	15505491	8469968	961560	7891142	76077586	1756.96	0.87	43300

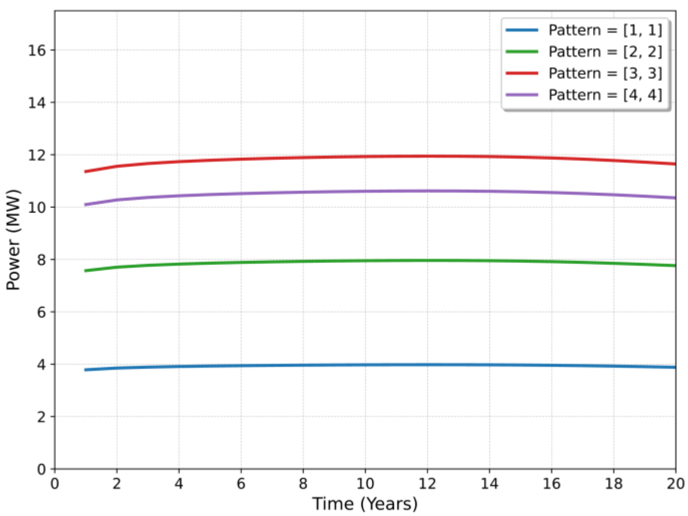

Figure 16. Net electric power of a single plant generated over time for various patterns in CPG systems. The total thermal power is equal to the number of power plants multiplied by the net power of each power plant shown here.

Subsurface simulations for this model were conducted using CMG, with the parameters outlined in Table 9 and Table 10. The design involves parallel fractures spaced within a distance of 1 km. The injection and production wellbores are vertically drilled to a depth of 4 km and extend 1 km horizontally to intersect all fractures (Figure 17). Four scenarios with varying fracture spacing and conductivity, as detailed in Table 11, were analyzed. The CMG simulation of the EGS system is integrated with a surface plant design similar to AGS within the TANGO framework.

Figure 18 and Figure 19 highlight critical performance trends: increasing fracture spacing leads to reduced power generation, while decreasing fracture conductivity similarly diminishes power output. This occurs because larger fracture spacing reduces the number of embedded fractures, thereby decreasing the heat exchange area. Cooler power consumption is negligible, nearly zero. However, in the CO_2 EGS system, the thermosiphon effect is relatively weak, making pump power the dominant energy consumer, with pump consumption approximately twice that of the condenser. In the most favorable scenario, the net power output reaches about 2.5 MW (as shown in Figure 19). To achieve a thermal power output of 10 MW, four EGS systems operating in parallel would be required.

Table 8. Key performance indicators for CO_2-Plume Geothermal systems with various patterns.

Pattern	Well CAPEX ($)	Permitting Capex ($)	Exploration CAPEX ($)	Surface gathering CAPEX ($)	Surface plant CAPEX ($)	Total CAPEX ($)	Net Electricity (KW)	LCOE ($/kWh)	SpCC ($/kW)
[1,1]	93884934	16547054	7717338	3846243	16221168	138216740	3934.41	0.71	35130
[2,2]	244100829	56971910	8199330	15384973	54125606	378782650	15737.63	0.48	24068
[3,3]	469424671	123622531	8836792	34616189	109610103	746110287	35409.68	0.42	21070
[4,4]	769856461	216498917	9629722.61	61539893	200904268	1258429262	62950.53	0.40	19990

DOI: 10.17185/duepublico/83331

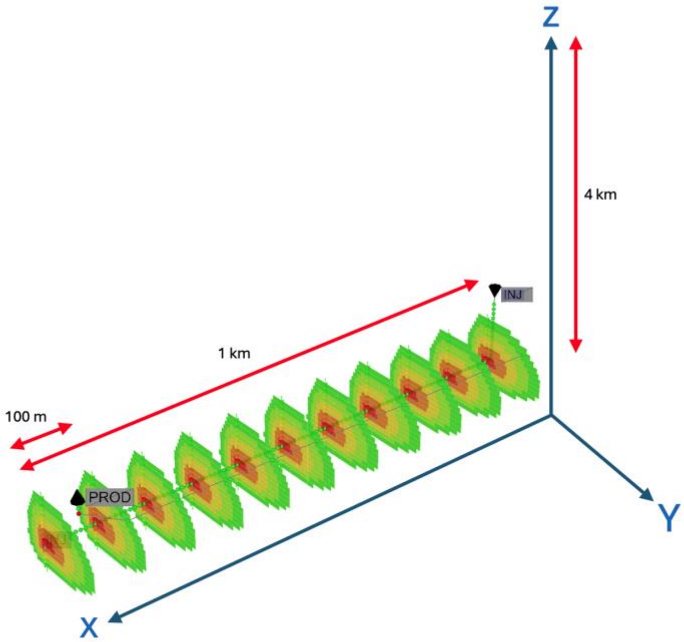

Figure 17. Fracture placement within the reservoir and the trajectory of horizontal wells are shown. The system depth is 4 km, and for the depicted system, 11 fractures are placed at equal intervals of 100 m.

Table 9. Base case surface/reservoir properties

Parameter	Value	Unit
average annual surface temperature	20	°C
Geothermal gradient	0.04	°C/m
Reservoir depth	4000	m
Reservoir thickness	100	m
Matrix porosity (uniform)	0.01	-
Matrix permeability (uniform)	0.1	mD
Rock density	2900	kg/m³
Rock thermal conductivity	2.8	W/(m°C)
Initial reservoir temperature	180	°C
Initial reservoir pressure	36000	kPa

Table 11. Scenario-specific parameters in EGS modeling

Scenario number	Fracture spacing (m)	Fracture conductivity (m-mD)
1	25	250
2	50	250
3	100	250
4	50	50

Table 10. Hydraulic fracturing and operational parameters

Parameter	Value	Unit
Horizontal well length	1000	m
Horizontal well spacing	150	m
Wellbore diameter	0.3	m
Fracture height	80	m
Fracture spacing	25, 50, 100	m
Fracture conductivity	50, 250	m-mD
Maximum injection BHP	115% overpressure	kPa
Target injection rate	100	kg/s
Minimum production BHP	40000	kPa

When comparing the LCOE values of EGS to those of CPG and hydrothermal systems, it becomes clear that EGS systems have a higher LCOE (Table 12). This is primarily due to the more extensive convective heat extraction mediums present in the CPG and hydrothermal systems, which enhance their efficiency. Furthermore, the flow rate in EGS systems is limited to 100 kg/s to reduce the risk of fracturing and significant seismic events. In scenarios with smaller fracture spacing and higher fracture conductivity, the LCOE values for EGS systems are lower.

5. CONCLUSION

This study provides a comprehensive evaluation of the potential to leverage power plant components and technology across diverse geothermal systems utilizing CO_2 as the working fluid, with the primary aim of reducing power plant costs, capital expenditures (CAPEX), and ultimately, the levelized cost of electricity (LCOE). By applying numerical tools within the

 DOI: 10.17185/duepublico/83331

TANGO framework, the net power generation, LCOE, and cost breakdowns for four geothermal systems—hydrothermal systems with CO_2 as a secondary working fluid, Advanced Geothermal Systems (AGS), Enhanced Geothermal Systems (EGS), and CO_2-Plume Geothermal (CPG) systems—were rigorously analyzed. This study also explores pathways to further cost reductions.

Key findings and their implications are as follows:

Advanced Geothermal Systems (AGS): While AGS demonstrates the potential to generate significant amounts of environmentally friendly electric and thermal power, the

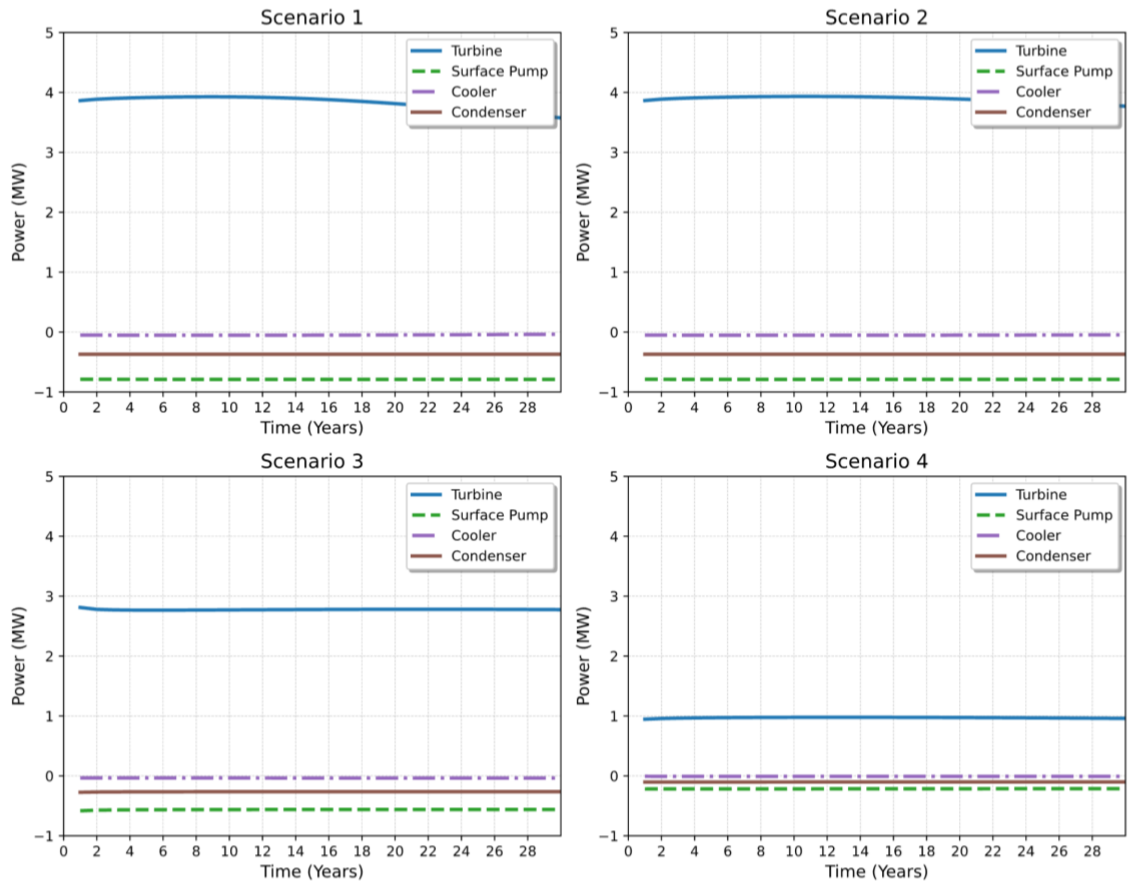

Figure 18. Power generation and consumption across surface plant components over time, analyzed for different scenarios addressed in Table 11.

Table 12. Key performance indicators for different scenarios addressed in Table 11.

Scenario	Well CAPEX ($)	Permitting Capex ($)	Exploration CAPEX ($)	Surface gathering CAPEX ($)	Surface plant CAPEX ($)	Total CAPEX ($)	Net Electricity (KW)	LCOE ($/kWh)	SpCC ($/kW)
1	33832816	11983338	5730124	961560	12468337	64976177	2617.75	0.46	24821
2	33832816	11983338	5730124	961560	12539511	65047352	2675.14	0.45	24315
3	33832816	11983338	5730124	961560	9792143	62299983	1913.55	0.61	32557
4	33832816	11983338	5730124	961560	4690519	57198360	644.84	1.65	88701

 DOI: 10.17185/duepublico/83331

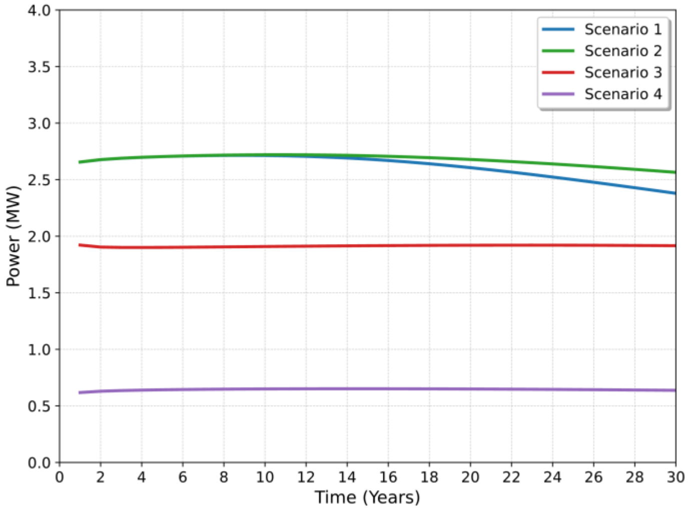

Figure 19. Net electric power generated over time for different scenarios addressed in Table 11.

LCOE remains prohibitively high, primarily due to substantial drilling costs. Simulations indicate that multilateral well designs could offer significant reductions in LCOE, but these remain insufficient for economic feasibility under current conditions. Promising advances in drilling technologies and operational optimization, however, could transform AGS into a cost-effective solution in the future.

Hydrothermal Systems with CO_2 as a Secondary Working Fluid: This novel concept benefits from CO_2-specific power plant components and shows promise in generating electric power. Although the single five-spot LCOE is higher than desired, strategies such as increasing flow rates and adopting multiple five-spot patterns yielded a substantial cost reduction, offering a pathway to enhanced economic viability.

CO_2-Plume Geothermal (CPG) Systems: CPG systems stand out for their dual benefits of power generation and CO_2 sequestration. Additional advantages include reduced pumping power requirements, the thermosiphon effect, and the direct injection of extracted fluid into turbines. Despite a slightly higher-than-desired LCOE for a single five-spot, increasing flow rates, expanding the number of five-spot patterns, using shared power plant components, and operating in brownfields have been identified as effective measures to achieve significant cost reductions, positioning CPG as a highly promising solution.

Enhanced Geothermal Systems (EGS): CO_2's superior mobility in fractured zones underscores its suitability as a working fluid in EGS. With high fracture conductivity and an increased number of effective fractures, LCOE values below 0.5 can be achieved, highlighting the economic promise of this approach under the right conditions.

A significant contributor to CAPEX across the systems evaluated is the surface plant cost, reaching up to 25% of total expenditures in hydrothermal, CPG, and EGS systems. Shared power plant components emerge as a pivotal factor in reducing these costs. However, for AGS systems, the surface plant cost contribution is comparatively minimal, typically less than 5%.

In conclusion, this study identifies both challenges and opportunities in the pursuit of economically viable geothermal energy solutions utilizing CO_2 as the working fluid. The findings underscore the importance of technological innovation, strategic design optimizations, and operational efficiencies to address current cost barriers. By leveraging these insights, future research and development efforts can advance the economic feasibility of these geothermal systems, contributing to the global transition toward sustainable and low-carbon energy sources.

6. REFERENCES

1. Favier A, Lardeaux JM, Corsini M, Verati C, Navelot V, Géraud Y, et al. Characterization of an exhumed high-temperature hydrothermal system and its application for deep geothermal exploration: An example from Terre-de-Haut Island (Guadeloupe archipelago, Lesser Antilles volcanic arc). Journal of Volcanology and Geothermal Research. 2021 Oct;418:107256.
2. Eyerer S, Schifflechner C, Hofbauer S, Bauer W, Wieland C, Spliethoff H. Combined heat and power from hydrothermal geothermal resources in Germany: An assessment of the potential. Renewable and Sustainable Energy Reviews. 2020 Mar;120:109661.
3. Ren Y, Kong Y, Pang Z, Wang J. A comprehensive review of tracer tests in enhanced geothermal systems. Renewable and Sustainable Energy Reviews. 2023 Aug;182:113393.
4. Asai P, Podgorney R, McLennan J, Deo M, Moore J. Analytical model for fluid flow distribution in an Enhanced Geothermal Systems (EGS). Renew Energy. 2022 Jun;193:821–31.
5. Moska R, Labus K, Kasza P. Hydraulic Fracturing in Enhanced Geothermal Systems—Field, Tectonic and Rock Mechanics Conditions—A Review. Energies (Basel). 2021 Sep 11;14(18):5725.
6. Esmaeilpour M, Gholami Korzani M, Kohl T. Evaluation of the Advantages of Multilateral Closed Deep Geothermal Frameworks over Conventional Geothermal Systems. In: Proceedings of the 47th Workshop on Geothermal Reservoir Engineering. Stanford, CA, USA; 2022.

 DOI: 10.17185/duepublico/83331

7. Esmaeilpour M, Gholami Korzani M, Kohl T. Performance Analyses of Deep Closed-loop U-shaped Heat Exchanger System with a Long Horizontal Extension. In: Proceedings of the 46th Workshop on Geothermal Reservoir Engineering. Stanford, CA, USA; 2021.
8. Esmaeilpour M, Gholami Korzani M, Kohl T. Stochastic performance assessment on long-term behavior of multilateral closed deep geothermal systems. Renew Energy. 2023 May;208:26–35.
9. Esmaeilpour M, Gholami Korzani M, Kohl T. Impact of thermosiphoning on long-term behavior of closed-loop deep geothermal systems for sustainable energy exploitation. Renew Energy. 2022 Jul;194:1247–60.
10. Brown CS, Falcone G. Investigating heat transmission in a wellbore for Low-Temperature, Open-Loop geothermal systems. Thermal Science and Engineering Progress. 2024 Feb;48:102352.
11. Duggal R, Rayudu R, Hinkley J, Burnell J, Wieland C, Keim M. A comprehensive review of energy extraction from low-temperature geothermal resources in hydrocarbon fields. Renewable and Sustainable Energy Reviews. 2022 Feb;154:111865.
12. Adams BM, Vogler D, Kuehn TH, Bielicki JM, Garapati N, Saar MO. Heat depletion in sedimentary basins and its effect on the design and electric power output of CO2 Plume Geothermal (CPG) systems. Renew Energy. 2021 Jul;172:1393–403.
13. Adams BM, Kuehn TH, Bielicki JM, Randolph JB, Saar MO. A comparison of electric power output of CO2 Plume Geothermal (CPG) and brine geothermal systems for varying reservoir conditions. Appl Energy. 2015 Feb;140:365–77.
14. Adams BM, Kuehn TH, Bielicki JM, Randolph JB, Saar MO. On the importance of the thermosiphon effect in CPG (CO2 plume geothermal) power systems. Energy. 2014 May;69:409–18.
15. Fleming MR, Adams BM, Ogland-Hand JD, Bielicki JM, Kuehn TH, Saar MO. Flexible CO2-plume geothermal (CPG-F): Using geologically stored CO2 to provide dispatchable power and energy storage. Energy Convers Manag. 2022 Feb;253:115082.
16. Hu Y, Cheng H, Tao S. Opportunity and challenges in large-scale geothermal energy exploitation in China. Crit Rev Environ Sci Technol. 2022 Nov 2;52(21):3813–34.
17. Kumar L, Hossain MdS, Assad MEH, Manoo MU. Technological Advancements and Challenges of Geothermal Energy Systems: A Comprehensive Review. Energies (Basel). 2022 Nov 30;15(23):9058.
18. Schifflechner C, de Reus J, Schuster S, Corpancho Villasana A, Brillert D, Saar MO, et al. Paving the way for CO2-Plume Geothermal (CPG) systems: A perspective on the CO2 surface equipment. Energy. 2024 Oct;305:132258.
19. swisstopo. 1st Caprock Integrity and Gas Storage Symposium 2024: Extended Abstracts. In: Ziegler M, Nicol R, Jaeggi D, Windisch J, Nussbaum C, editors. 1st Caprock Integrity and Gas Storage Symposium. St-Ursanne, Switzerland: swisstopo; 2024.
20. Brown DW. A hot dry rock geothermal energy concept utilizing supercritical CO2 instead of water. In: Proceedings of the twenty-fifth workshop on geothermal reservoir engineering. Stanford University; 2000.
21. Permann CJ, Gaston DR, Andrš D, Carlsen RW, Kong F, Lindsay AD, et al. MOOSE: Enabling massively parallel multiphysics simulation. SoftwareX. 2020 Jan;11:100430.
22. Gaston D, Newman C, Hansen G, Lebrun-Grandié D. MOOSE: A parallel computational framework for coupled systems of nonlinear equations. Nuclear Engineering and Design. 2009 Oct;239(10):1768–78.
23. Esmaeilpour M, Nitschke F, Kohl T. GenEOS: An accurate equation of state for the fast calculation of two-phase geofluids properties based on gene expression programming. Comput Phys Commun. 2024 Apr;297:109068.
24. Asai P, Panja P, McLennan J, Deo M. Effect of different flow schemes on heat recovery from Enhanced Geothermal Systems (EGS). Energy. 2019 May;175:667–76.
25. Adams B, Ogland-Hand J, M. Bielicki J, Schädle P, Saar M. Estimating the Geothermal Electricity Generation Potential of Sedimentary Basins Using genGEO (The Generalizable GEOthermal Techno-Economic Simulator). 2021.

 DOI: 10.17185/duepublico/83331

DOI: 10.17185/duepublico/83331
URN: urn:nbn:de:hbz:465-20250428-105325-6